JOURNAL OF SPACECRAFT AND ROCKETS
Vol. 30, No. 1, January–February 1993

New Approximate Method for Calculating Real Gas Effects on Missile Configurations

F. G. Moore,* M. J. Armistead,† and S. H. Rowles†
Naval Surface Warfare Center Dahlgren Division, Dahlgren, Virginia 22448
and
F. R. DeJarnette‡
North Carolina State University, Raleigh, North Carolina 27695

New methods have been developed to compute inviscid surface pressures and temperatures for both perfect and equilibrium chemically reacting flows on pointed and blunt bodies of revolution. These new methods include an improved shock-expansion theory, an improved modified Newtonian theory, and an improved method for angle-of-attack effects. Comparison of these approximate engineering techniques to inviscid computations using a full Euler code showed that these new methods gave very good agreement of inviscid surface temperature and pressures as well as forces and moments. Incorporation of this new technology into the Naval Surface Warfare Center Dahlgren Division aeroprediction code will allow the code to be used for engineering estimates of inviscid surface temperature at high Mach numbers. These approximate temperatures can then be used as inputs to perform heat transfer analysis.

Nomenclature

a = speed of sound, ft/s
C = pressure coefficient
C_{po} = pressure coefficient at stagnation point
d = body diameter, ft; one body diameter = 1 caliber
e = internal energy, ft^2/s^2
H = total enthalpy, ft^2/s^2
h = specific enthalpy, ft^2/s^2
L = body length, calibers
M = Mach number
p = pressure, lb/ft^2
R = gas constant, for air = 1716 ft-lb/(slug-°R)
R_N = nose radius
S = distance along body surface, ft
T = temperature, °R
V = velocity, ft/s
x = distance along body axis of symmetry, ft
Z = compressibility factor, $p/\rho RT$ (= 1 for perfect gas)
α = angle of attack, deg
β = $\sqrt{M^2-1}$
γ = ratio of specific heats
δ_{eq} = angle between velocity vector and a tangent to the body at a given point on surface
η, η_1 = exponent or factor used in shock-expansion theory
θ = local body slope with respect to axis of symmetry
λ = $\rho V^2/\beta$
μ = Mach angle, = $\sin^{-1}(1/M)$
ρ = density
Φ = roll angle where $\Phi = 0$ deg is leeward plane

Subscripts

c = cone
o = total conditions
∞ = freestream conditions
1, 2 = conditions before and after a point on body surface, respectively

Received June 4, 1992; revision received Sept. 1, 1992; accepted for publication Sept. 3, 1992.

*Staff Scientist, Weapons Systems Department. Associate Fellow AIAA.
†Aerospace Engineer, Aeromechanics Branch.
‡Professor, Mechanics/Aerospace Department. Associate Fellow AIAA.

Introduction

OVER the past 20 years, many weapon concepts have been investigated with various versions of the Naval Surface Warfare Center Dalgren Division (NSWCDD) aeroprediction code.[1-4] During the last 10 years, several of the concepts had regions of flight or designs that were outside of the range of the latest version of the code produced in 1981.[4] As a result, a recent review of computational aerodynamics at NSWCDD[5] recommended that the latest version of the code be upgraded to allow Mach numbers up to 20, to incorporate a nonlinear lift prediction capability with emphasis on very low aspect ratio dorsals, and to expand the empirical base drag data base so improved estimates of this drag component as a function of angle of attack, fin location, and size could be made. All three of these efforts are currently underway. This paper deals with the first of those objectives, extending the Mach number capability from 8 up to at least 20.

The main reason the fourth version[4] of the aeroprediction code was limited to Mach number 8 was that, above $M_\infty = 6$, real gas effects start becoming important and can still be neglected at $M_\infty = 8$. However, as Mach number increases substantially above $M_\infty = 6$, the need to include real gas effects into the aeroprediction code increases if one is interested in inviscid surface temperatures. If one is only interested in forces and moments, real gas effects have a slight effect on the pitching moment but only second-order effects on axial and normal force.[6] However, one of the key issues in high-speed vehicles is aerodynamic heating, material selection, and insulation. Any excess weight can have a strong adverse impact on vehicle performance. Thus, a simple yet accurate method of estimating vehicle surface temperature (inviscid) for use in heat transfer analysis is needed.

The theoretical methodology used in the present code to predict aerodynamics above about Mach 3 is second-order shock-expansion theory (SOSET) combined with modified Newtonian theory (MNT). A brief search of the literature revealed no current second-order (or even comprehensive first-order) accurate theoretical techniques for including real gas

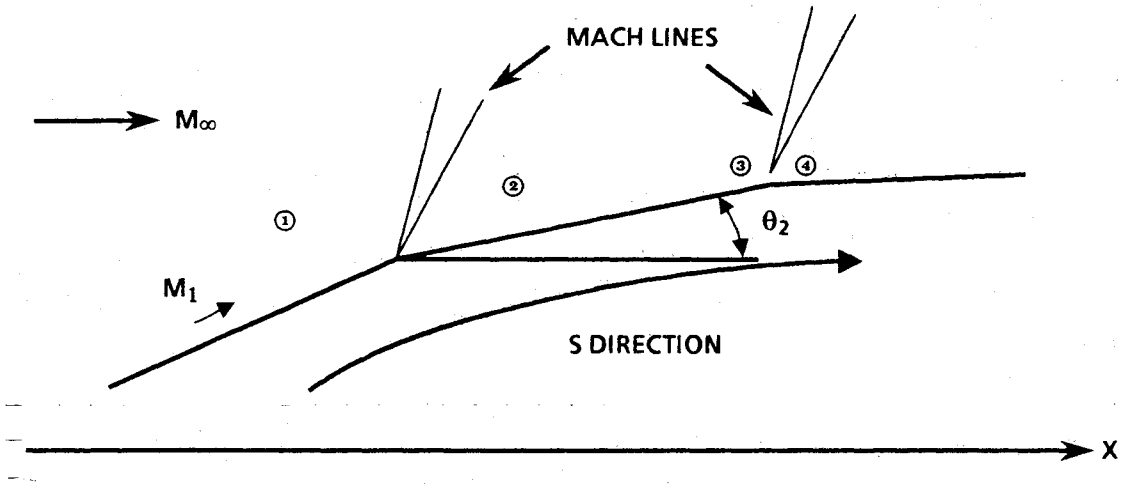

Fig. 1 Flow about a frustum element.

effects into aerodynamic computations. The only approaches available were either incorporation of real gas effects into the full inviscid Euler equations of motion or first-order local slope techniques. The first approach is beyond the computational complexity desired for an approximate engineering code, whereas the latter approach does not in general yield accurate axial force calculations. Even for a first-order local slope approach, a robust code that gives accurate forces and moments as well as local temperatures with real gas effects included was not found. The closest thing to this is the current code used at NSWCDD and elsewhere for computing heat transfer coefficients called MINIVER.[7]

This paper will summarize the key ingredients of a new approach for calculating inviscid surface pressures, temperatures, forces, and moments in an equilibrium chemically reacting flow. The new technology includes 1) an improved shock expansion theory for real gas effects, 2) an improved MNT including real gas effects, and 3) an improved method for including angle-of-attack effects over that which exists in the current code.

The inviscid temperature referred to is that at the edge of a boundary layer that is thin relative to the body and shock layer. If the boundary layer is not thin (fully viscous shock layer) or the entropy layer is swallowed by the boundary layer, other means must be used to estimate the boundary-layer edge temperatures.

Analysis

This section will briefly summarize the theoretical methodology without details of the derivation. Interested readers are referred to an NSWCDD technical report[8] that has all of the details of the theoretical derivations as well as a summary of state-of-the-art real gas solutions and a brief tutorial on real gas effects. The section is divided into the three areas where it is believed new additions to the state of the art are made. These areas are: 1) a simplified method for computing accurately real gas effects on bodies of revolution, 2) a new improvement to MNT, and 3) a new improved angle-of-attack method.

Extension of Shock Expansion and Modified Newtonian Theories to Include Real Gas Effects

The SOSET is given by

$$p = p_c - (p_c - p_2)e^{-\eta} \tag{1}$$

where η is an exponential decay term given by

$$\eta = \frac{(\partial p/\partial s)_2(s - s_2)}{p_c - p_2} \tag{2}$$

Refer to Fig. 1 for the nomenclature.

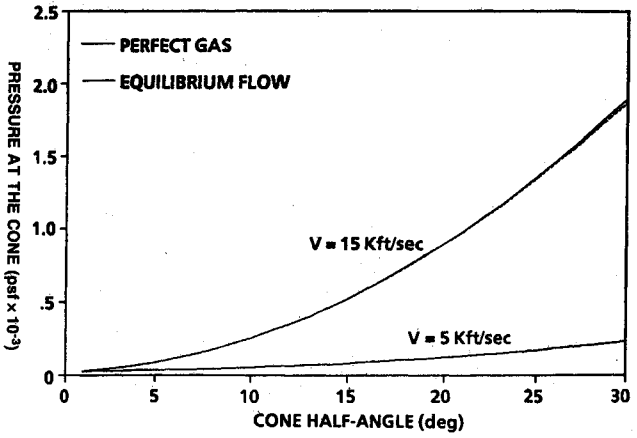

Fig. 2a Effect of freestream velocity and cone half-angle on cone surface pressure (H = 100,000 ft).

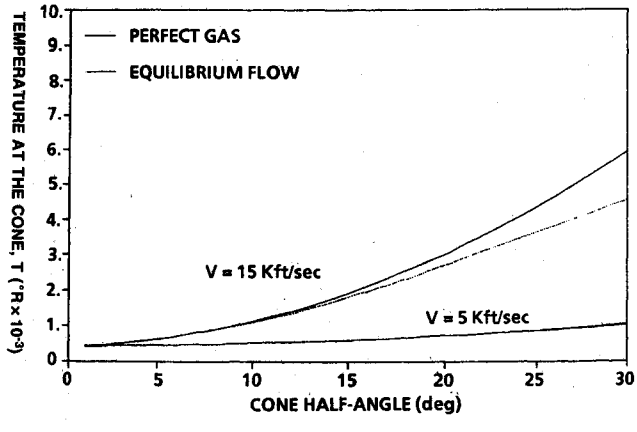

Fig. 2b Effect of freestream velocity and cone angle on cone surface pressure (H = 100,000 ft).

Here η is positive. If conditions are such that η becomes negative, then Eq. (1) does not satisfy the boundary conditions of $p = p_c$ as $s \to \infty$ and therefore η must be defined by an equation different from Eq. (2). A value of $\eta = 0$ causes the SOSET to revert back to generalized shock expansion theory; a value of η between $\eta = 0$ and ∞ allows a blend of these two theories. To extend SOSET to real gases requires several things: 1) a cone solution for real gases (p_c), 2) a Prandtl-Meyer expansion (PME) for real gases (p_2), and 3) a derivation of a new pressure derivative $(\partial p/\partial s)_2$ where the perfect gas

assumption has not been made, and 4) a way to compute temperature given values of pressure.

The cone solution and PME for real gases have been done and are standard in the literature.[9,10] These methods have been implemented into the aeroprediction code. Typical results of the cone and expansion process for pressure and temperature are given in Figs. 2 and 3. Note that for compression processes, pressure is practically unaffected by real gas effects whereas temperature is lowered due to the sharing of the translational energy of molecules and atoms with the vibration, dissociation, rotation, and electronic excitation modes of internal energy. On the other hand, both pressure and temperature are impacted in expansion processes (Fig. 3).

To compute the pressure gradient behind a corner in a chemically reacting flow with Eq. (2) for use in the SOSET requires several steps: 1) conversion of the full Euler equations of motion from rectangular to streamline coordinates and then derivation of the characteristic equations, 2) derivation of the pressure change along a left running characteristic or Mach line since this is the mechanism for differential pressure change along the surface, and 3) an algebraic approximation to the solution of an ordinary differential equation.

The final result of this process is (see Ref. 8)

$$\left(\frac{\partial p}{\partial s}\right)_2 = \frac{F_3 + F_4}{F_5 - F_1/2\lambda_2} \tag{3}$$

where

$$F_1 = \left\{\left[\frac{\rho_1 V_1 \sin(\mu_1)}{\rho_2 V_2 \sin(\mu_2)} - 1\right]^2 + (\mu_1 + \theta_1 - \mu_2 - \theta_2)^2 \left[\frac{\rho_1 V_1 \sin(\mu_1)}{\rho_2 V_2 \sin(\mu_2)}\right]^2\right\}^{1/2}$$

$$F_2 = \frac{\rho_1 V_1 \sin(\mu_1)}{\rho_2 V_2 \sin(\mu_2)}$$

$$F_3 = \frac{1}{2\lambda_1}\left(\frac{\partial p}{\partial s}\right)_1 [F_1 + 4\cos(\mu_1)]$$

$$F_4 = (1/r)[\sin(\mu_1)\sin(\theta_1) - F_2 \sin(\mu_2)\sin(\theta_2)]$$

$$F_5 = F_2\left[\frac{2\cos(\mu_2)}{\lambda_2}\right]$$

$$\lambda = \frac{\rho V^2}{\sqrt{M^2 - 1}}$$

$$\mu = \sin^{-1}\frac{1}{M}$$

and where subscripts 1 and 2 refer to before and after a turn as illustrated in Fig. 1. No perfect gas assumption was made in the derivation of Eq. (3). Equations (1-5), along with cone and PME solutions discussed earlier, allow computation of pressure in equilibrium chemically reacting flows on pointed bodies of revolution at zero angle of attack using SOSET.

For blunt bodies, MNT was extended to include real gas effects. The MNT pressure coefficient is given by

$$C_p = C_{p_o} \sin^2(\delta_{eq}) \tag{4}$$

For perfect gases, C_{p_o} can be found by using normal shock tables.[11] However, for real gases, the normal shock solution is an iterative process.[12] Once the normal shock solution has been generated, values of γ_2, p_2, ρ_2, h_2, a_2, V_2, M_2, T_2, Z_2, and S_2 just behind the shock are known or can be computed from appropriate thermodynamic relations. To take the properties behind the shock to the stagnation point, it is assumed that and γ_2 and Z_2 are constant.

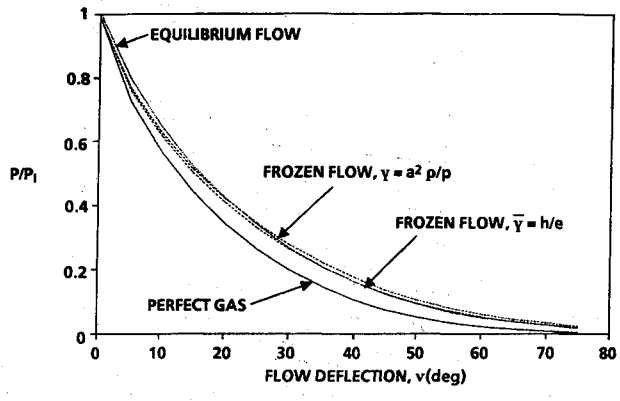

Fig. 3a Perfect, frozen, equilibrium PME; pressure vs flow deflection angle ($M_1 = 1.0$, $T_1 = 6140$ K, $p_1 = 1.2$ atm).

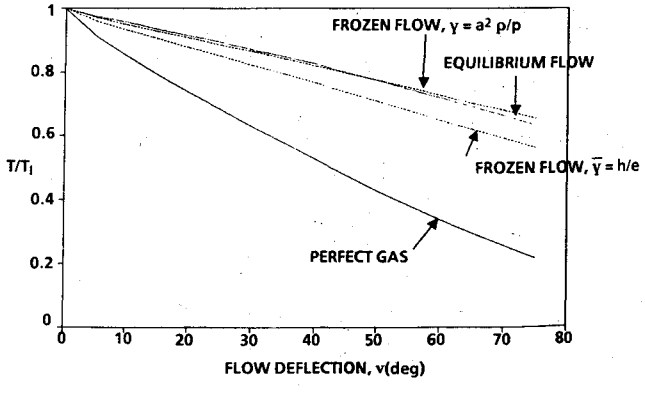

Fig. 3b Perfect, frozen, equilibrium PME: temperature vs flow deflection angle ($M_1 = 1.0$, $T_1 = 6140$ K, $p_1 = 1.2$ atm).

indicated a maximum of 2.3% error in making this assumption, and in most cases the error was much less. Also, since velocity and Mach number are zero at the stagnation point, the static temperature, pressure, density, and enthalpy at the stagnation point are simply the total values behind the shock. Now to continue the computation around the body surface to where SOSET is applied, Eq. (4) is applied and then the local pressure at the point in question is simply

$$p_L = p_\infty\left(1 + \frac{\gamma_\infty M_\infty^2}{2} C_p\right) \tag{5}$$

Equations (1-5) now allow the computation of pressures all around a blunt or pointed body of revolution at zero angle of attack.

To compute inviscid temperatures (and other properties) along the surface of a pointed or blunt body, use is made of the constancy of entropy along the surface for perfect, frozen, or equilibrium chemically reacting flows. Knowing the value of entropy and pressure from the pointed cone solution of Ref. 9 or the normal shock solution of Ref. 12 for a blunt body, one can then use the thermofit equations of Refs. 13 and 14 to determine other properties. That is,

$$T = T(p,s) \tag{6a}$$

$$\rho = \rho(p,s) \tag{6b}$$

$$a = a(p,s) \tag{6c}$$

$$e = e(p,s) \tag{6d}$$

The remaining properties at the body surface can be found from standard thermodynamic relationships. That is,

$$h = e + p/\rho \tag{7a}$$

$$H = (\gamma_\infty R/\gamma_\infty - 1)T_{o_\infty} = \text{const} \tag{7b}$$

$$V = \sqrt{2(H-h)} \tag{7c}$$

$$M = V/a \tag{7d}$$

$$\gamma = a^2\rho/p \tag{7e}$$

$$Z = p/\rho RT \tag{7f}$$

Improved Version of Modified Newtonian Theory (MNT)

To get an accurate pressure over the entire body using SOSET requires an accurate starting solution. The last author recognized that in comparing MNT pressures with those of an exact Euler solver,[15] MNT overpredicted pressure for $M_\infty > 3.5$ and $X/R_N < 0.5625$ and underpredicted pressure for most of the region $X/R_N > 0.5625$. However, the MNT predicted the correct pressure at $X/R_N = 0.5625$ for $3.5 < M_\infty \leq 30$. As a result, he was able to derive a change in the MNT given by

$$\Delta C_p = k \cos^m(\delta_{eq}) \left[\cos \delta_{eq} - \cos(\delta_{eq})_M\right] \tag{8}$$

so that the new C_p is given by

$$C_p = (C_p)_{\text{MNT}} - \Delta C_p \tag{9}$$

Here, $(\delta_{eq})_M = 25.95$ deg, $m - 2.78$, and

$$k = -2.416C_{p_o} + 4.606[0.1507C_{p_o}^2 + (1.124/M_\infty^2)C_{p_o}]^{1/2}$$

Here subscript M refers to the match point being MNT and SOSET. Again, the interested reader is referred to Ref. 8 for the details of this derivation.

Improved Angle-of-Attack Solution

As already mentioned, it is very critical to have an accurate starting solution for both blunt and pointed bodies. For pointed bodies, Ref. 16 gave a solution for the conical tip of

$$C_p(\alpha,\Phi) = C_{p_{\alpha=0}} - \sin(2\alpha)\sin(2\theta_c)\cos(\Phi) + F\sin^2(\alpha)\cos^2(\theta_c) \tag{10}$$

where

$$F = (2 - 1/\beta)(1 - \tan^2\theta_c) - (2 + 2/\beta)\sin^2\Phi$$

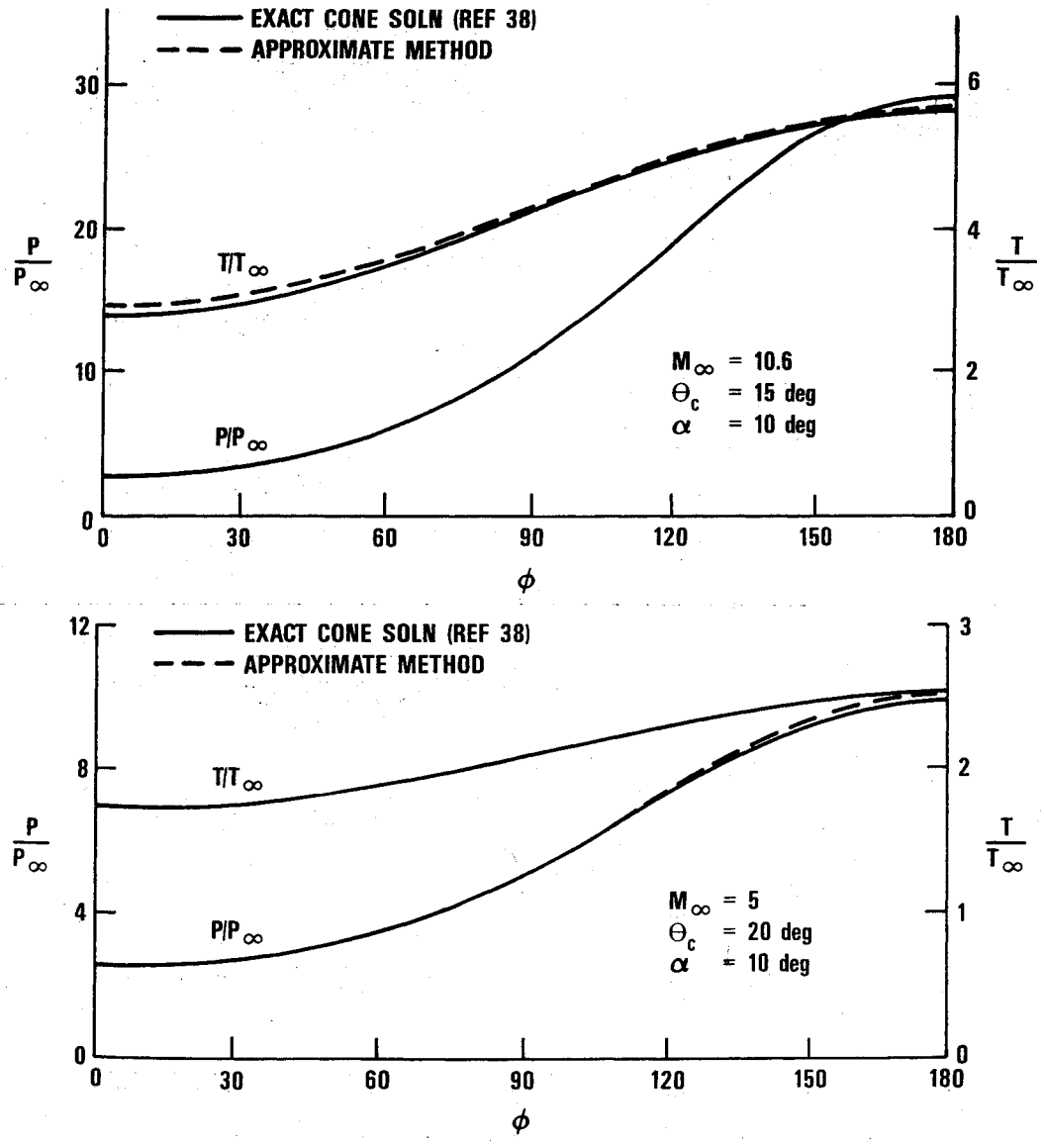

Fig. 4 Perfect gas comparisons of exact and present approximate cone solutions.

A new and slightly improved solution over Eq. (10) is

$$C_p(\alpha,\Phi) = C_{p_{\alpha=0}} - (2\alpha)\sin(2\theta)\cos(\Phi) + (F\cos^2\theta)\alpha^2 + [4/3\sin(2\theta)\cos(\Phi)]\alpha^3 \quad (11)$$

The $C_{p_{\alpha=0}}$ comes from the real gas solution for cones at $\alpha = 0$. Equation (11) was derived by using Eq. (10) in a Taylor series expansion.[8] Reference 9 gave an approximate formula for $C_{p_{\alpha=0}}$, which is accurate to less than 1.5%. That is,

$$C_{p_{\alpha=0}} = 2/\gamma_\infty M_\infty^2[1.4932(M_\infty \sin\theta_c)^{1.9854} + 0.3017] \quad (12)$$

To get temperature and other properties around the cone or pointed body of revolution, recall that entropy on the body is constant for equilibrium chemically reacting flows and equal to that in the windward plane ($\Phi = 180$ deg). To get this value, we use the following procedure:

1) Solve Eq. (11) for C_p at $\Phi = 180$ deg using the cone angle at the nose tip.

2) Use Eq. (12) to solve for the value of θ_c corresponding to the value of C_p from step 1.

3) Use this new value of θ_c to solve for the real gas cone solution of Ref. 9. This gives entropy and other flow properties in the windward plane.

4) Using this value of entropy and the value of C_p from Eq. (11), compute the value of temperature and other properties around the surface from Eqs. (6) and (7) (here θ is the angle at the nose tip).

This simplified approach given by Eq. (11) is also applied downstream on both pointed and blunt bodies except that the value of θ is the local slope on the body surface. Also, $C_{p_{\alpha=0}}$ is the zero angle-of-attack solution provided by the improved MNT combined with the shock expansion theory or the conical starting solution combined with shock expansion theory. Accurate blunt body starting solution values of properties have already been discussed.

For pressure predictions aft of blunt-nosed sections, it was found that a more accurate pressure prediction in the leeward plane area ($\Phi \leq 30$ deg) could be made from

$$C_p(\alpha,\Phi) = C_{p_{\alpha=0}} - \frac{(2\alpha)\sin(2\theta)\cos(\phi)}{3} \quad (13)$$

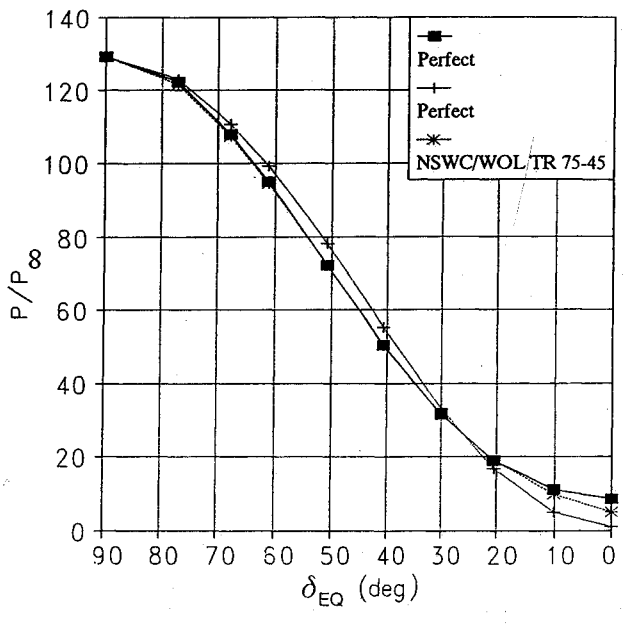

Fig. 5 Surface pressure distribution over a hemispherical forebody at $M_\infty = 10$.

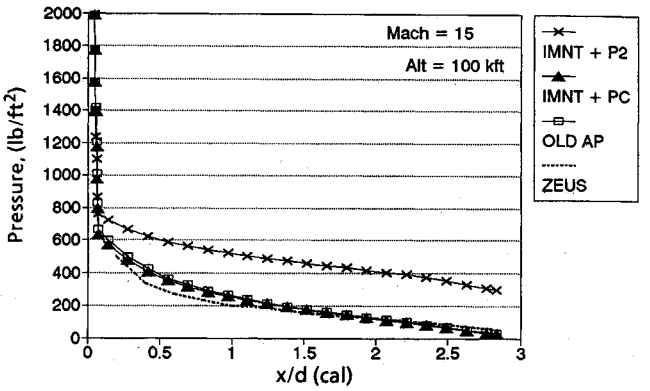

Fig. 6 Comparison of various pressure prediction techniques on a 20% blunt von Kármán ogive ($M_\infty = 15$, $\alpha = 0$ deg, alt = 100,000 ft).

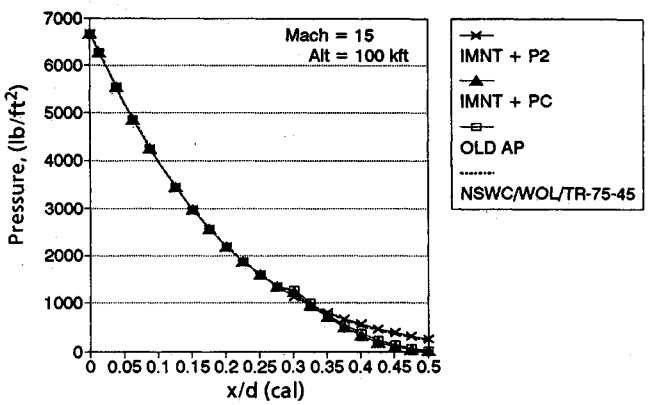

Fig. 7 Comparison of various pressure prediction techniques on a hemisphere forebody ($M_\infty = 15$, $\alpha = 0$, alt = 100,000 ft).

For the afterbody portion behind the shoulder of the nose-afterbody junction, MNT is used all around the body. That is,

$$C_p = C_{p_o}\sin^2(\delta_{eq}) \quad (14)$$

If $\delta_{eq} \leq 0$, $\delta_{eq} \equiv 0$ so that in the shadowed regions of flow C_p is defined as zero according to the Newtonian theory. In summary, angle-of-attack solutions are generated by Eqs. (11), (13), and (14) along with the procedure described to obtain entropy and the zero angle-of-attack solution. Then knowing pressure and entropy, other properties are calculated from Eqs. (6) and (7).

Results and Discussion

Before the new methods were applied to real gas computations, several questions were addressed for perfect gases: 1) The accuracy of the starting solutions for pointed and blunt-nosed bodies, 2) the value of η in Eq. (2) and the most appropriate value for high Mach number configurations, and 3) the behavior of Eq. (11) in the leeward plane of blunt-nosed configurations.

To address question 1, perfect gas computations were made using the present approximate techniques and compared with solution of the full inviscid equations of motion for cones[17] and spheres.[15] Typical results for cones are shown in Fig. 4 for pressure and temperature and for hemispheres in Fig. 5. No exact solution data were available in Ref. 15 for temperature, but both Figs. 4 and 5 show excellent agreement on pressure for cones and hemispheres and good agreement on cone temperature. Although comparisons are not shown in the paper, Ref. 8 shows that the good agreement shown in Figs. 4 and 5 of the approximate cone and improved modified Newtonian

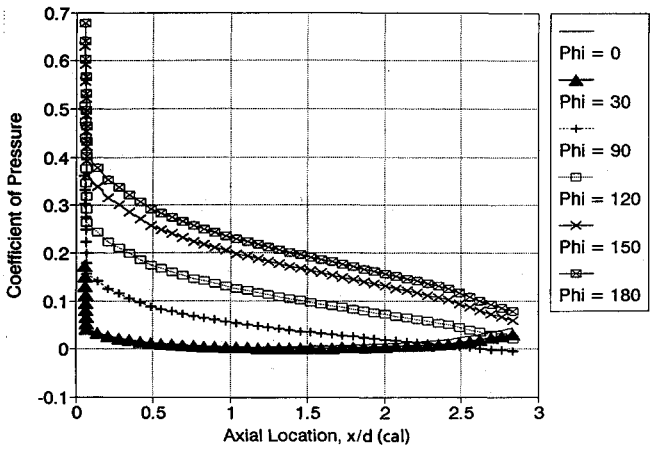

Fig. 8 Approximate pressure coefficients on 20% blunt von Kármán ogive on various Φ planes [$M_\infty = 15$, $\alpha = 10$, perfect gas, Eq. (11) only].

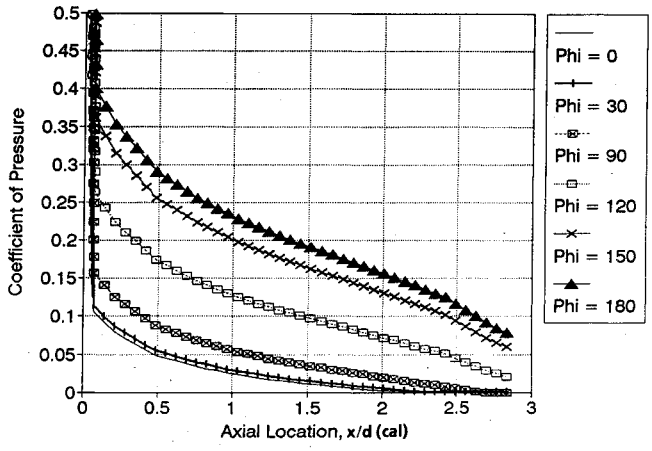

Fig. 9 Approximate estimate of pressure on 20% blunt von Kármán ogive [$M_\infty = 15$, $\alpha = 10$, perfect gas, Eqs. (11) and (13)].

theory (IMNT) compared with exact computations holds over a wide range of angles of attack, Mach numbers, and cone angles. Also, the aerodynamic coefficients are accurate to within 2% of the exact values. This degree of accuracy for the starting solutions should allow improved accuracy of surface properties downstream.

To address the value of η computed by Eq. (4) and used in Eq. (2), several cases were investigated for various Mach numbers. It was found that, as Mach number increases, η becomes negative most of the time and as a result SOSET is replaced by generalized shock expansion theory (GSET) or tangent cone theory (TCT) depending on the value of η. However, examining GSET compared with exact solution results[18] on two cases (20% blunt von Kármán ogive and a hemisphere) revealed that this is not the best option for η in all cases. To illustrate this, consider Figs. 6 and 7, which are plots of pressure vs distance down the body. Results in each figure include full Euler solutions, the old aeroprediction code results, and the new aeroprediction results with limiting values of η. The limiting values of η are where $\eta = 0$, which means SOSET reverts to GSET (IMNT + P_2), and when $\eta = \infty$, which means SOSET reverts back to tangent cone (IMNT + P_c). Note that for the hemisphere forebody the IMNT plus GSET (IMNT + P_2) agrees more closely with the exact solution than does the old aeroprediction code or IMNT plus tangent cone (IMNT + P_c). However, for the blunt von Kármán ogive just the opposite was true. Hence, it was concluded that a better alternative to setting $\eta = 0$ or ∞ automatically in the code when $\partial p/\partial s$ was negative was to allow η to be input by the user. This would allow the best estimate of pressure on all configurations since p_2 and p_c were available in the aeroprediction code.

Equation (1) was therefore revised for Mach numbers greater than 6 to

$$p = p_c - (p_c - p_2)\eta_1$$

Here $\eta_1 = 0$ gives $p = p_c$ and $\eta_1 = 1$ gives $p = p_2$. Based on Figs. 6 and 7, it is recommended that a value of η_1 near 0 be used for slightly blunt ogives or cones and a value of η_1 near 1 be chosen for large bluntness on the nose.

To address question 3, consider Figs. 8 and 9. Figure 8 contains the pressure computations using only Eq. (11) for several planes around the body. Although the exact computations are not shown for clarity, good agreement between the approximate and exact techniques are obtained for $\Phi > 30$ deg. A slight exception to this statement is in the overexpansion region near the blunt tip. On the other hand, the Eq. (11) results in the leeward plane show unacceptable behavior (Fig. 8, $\Phi = 0$, 30 deg). This is because Eq. (11), although excellent for cones at all values of Φ, underpredicts pressures in the overexpansion region of the leeward plane area on a blunt-nosed body and overcompensates for this near the shoulder of the body. To remedy this, Eq. (11) was modified according to Eq. (13) for $\Phi \leq 30$ deg on blunt-nosed configurations. Figure 9 presents the results of this modification. As seen in the figure, results are more reasonable on all planes around the body. Note that defining $C_p = 0$ when it goes negative ($X > 2.2$) will also have the effect of putting a lower limit on temperature. Although ZEUS results are not shown for clarity purposes on Fig. 9, they agree much closer with the approximate results than the use of Eq. (11) alone. Use of Eq. (13) in conjunction with Eq. (11) improves the normal force and center of pressure prediction by 5 and 6%, respectively, over Eq. (11) alone while not affecting the accuracy of C_A.

All calculations presented up to this point have been for perfect gases. To compare the approximate methods shown herein with solution of the Euler equations for real gases, several test configurations were derived typical of missile configurations or body components. These configurations are shown in Fig. 10. They consist of a 20% blunt von Kármán ogive, a 20% blunt cone, a sharp cone-cylinder-flare, and a 20% blunt von Kármán ogive-cylinder-fin configuration.

Figure 11 presents the perfect and equilibrium chemically reacting flow temperature results for the 20% blunt von Kármán ogive using the present method and compared with the numerical solutions of the full Euler equations. Only three planes are shown for clarity. Note that excellent agreement between the approximate and exact results are obtained (Fig. 11b). In the critical windward plane, agreement is within about 3% all along the surface. Although pressure comparisons are not shown, the same trends on agreement with ZEUS code results are obtained.[8] Also of interest is to compare the perfect gas and real gas temperatures in Figs. 11a and 11b. The real gas temperatures in the critical windward plane are lower by as much as a factor of two, thus illustrating why a perfect gas cannot be assumed when one is interested in inviscid surface temperatures at very high Mach number. This is particularly true in the region of large slopes (near the blunt tip, large cone, or wedge angles, etc.).

Figure 12 further illustrates the point made earlier about perfect vs real gas computations. Figure 12 is the windward plane inviscid surface temperature on a 20% blunt cone with half-angle 15 deg at $M_\infty = 15$ and $\alpha = 10$ deg (second case of Fig. 10). Again, full Euler and approximate results are shown for both perfect and real gas computations. The real gas temperatures along the constant slope portion of the blunt cone are only about 60% of the perfect gas results. Figure 12

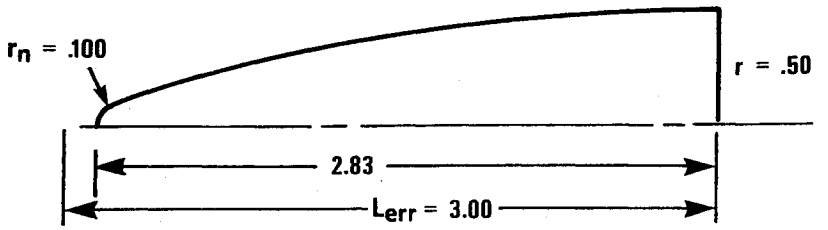

TEST CASE 1 20% BLUNT VONKARMON OGIVE

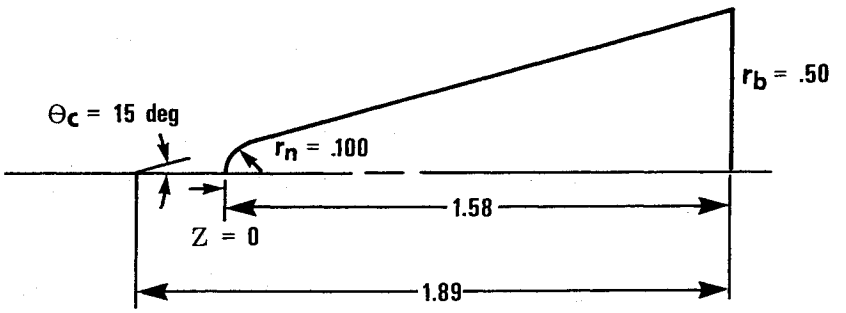

TEST CASE 2 20% BLUNT CONE

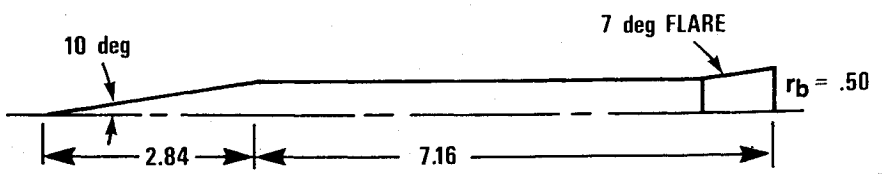

TEST CASE 3 CONE - CYLINDER - FLARE

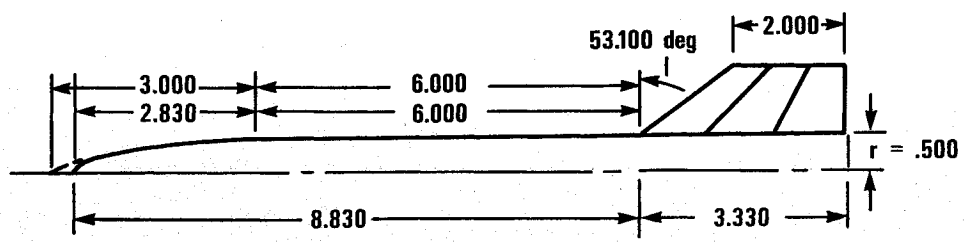

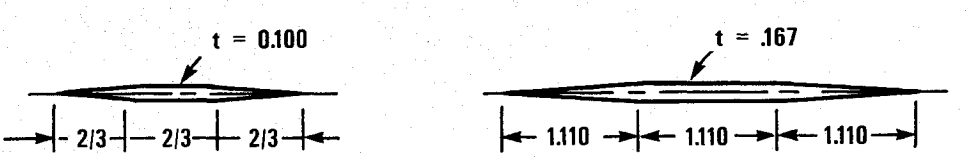

WING TIP CROSS SECTION WING ROOT CROSS SECTION

TEST CASE 4 : 20% BLUNT VONKARMON OGIVE
CYLINDER WITH CRUCIFORM TAILS

Fig. 10 Configurations used as test cases for new theory (dimensions in calibers).

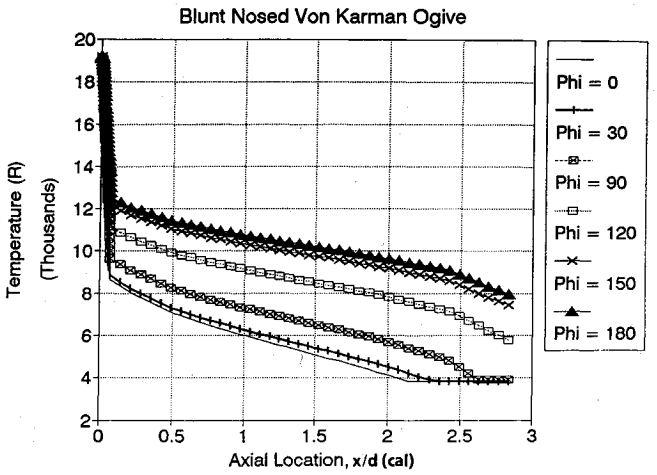

Fig. 11a Approximate temperature prediction on a 20% blunt von Kármán ogive ($M_\infty = 15$, $\alpha = 10$ deg).

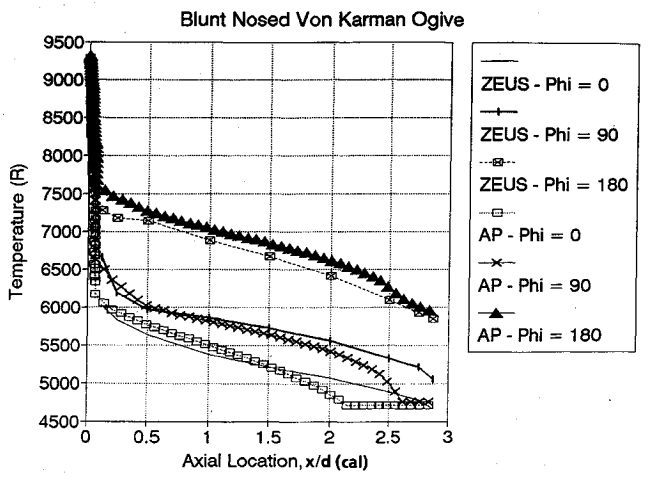

Fig. 11b Comparison of approximate and exact temperature prediction on a 20% blunt von Kármán ogive for a real gas ($M_\infty = 15$, $\alpha = 10$ deg, alt = 100,000 ft).

presents the pressure and temperature on this same 20% blunt, 15 deg half-angle cone as a function of Mach number. Real and perfect gas approximate solutions are given for $\alpha = 0$ and 15 deg. Full Euler results are shown for $M_\infty = 15$ deg only.

The results presented are those near the base of the cone, $x = 1.5$, and in the windward plane. Several points are worthy of note. First of all, Fig. 12b reiterates the negligible effect of real gas conditions on pressure at all Mach numbers. It also illustrates the strong pressure increase as a function of angle of attack and Mach number. Figure 12c illustrates how the real gas affects temperature as Mach number increases. It is also interesting to note that, although temperature differs by up to several thousands of degrees due to angle-of-attack effects for a perfect gas, the real gas difference is a maximum of 1500°R at $M_\infty = 20$ and $\alpha = 15$ deg. Finally, as already discussed, the present approximate code gives very good agreement for inviscid surface properties with the full Euler solver, ZEUS, except in the overexpansion region behind the nose tip.

The third case considered is a cone-cylinder-flare configuration (see Fig. 10). Results of the temperatures on this configuration are shown in Fig. 13, which presents the temperature in the windward plane as a function of distance along the body surface. Note that the present theory shows no overexpansion behind the shoulder because MNT is used to estimate pressures around the surface. Also note that for the conical surfaces, real gas temperatures are lower by only about 10–15%, whereas on blunt-nosed configurations at the same Mach number, temperatures can be as much as a factor of two lower for real compared with perfect gases.

The final case considered is the 20% blunt von Kármán ogive-cylinder-fin configuration shown in Fig. 10. The angle-of-attack 0-deg temperature for real and perfect gases is shown in Fig. 14 for $M_\infty = 15$. Note again the excellent agreement up to the location of the tail fins. This figure was primarily shown to indicate that, although the current approximate engineering code is quite applicable for preliminary design, it does not

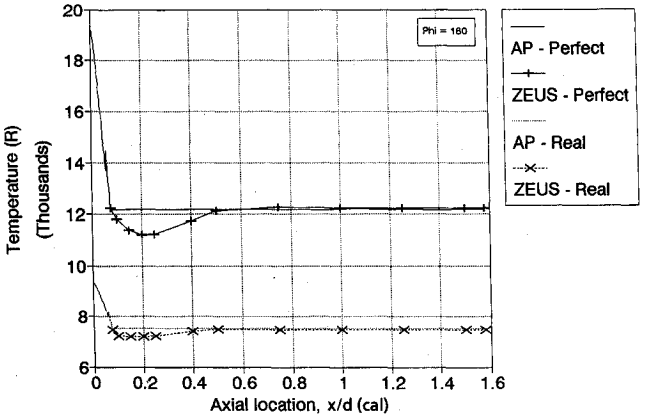

Fig. 12a Comparison of approximate and exact temperature in the windward plane of a 20% blunt cone ($M_\infty = 15$, $\alpha = 10$ deg, alt = 100,000 ft).

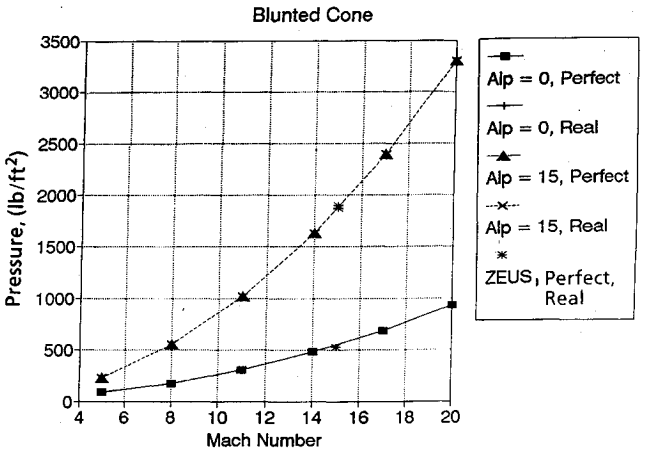

Fig. 12b Pressure predicted by approximate method on a 20% blunt cone as a function of Mach number ($M_\infty = 15$, $\Phi = 180$ deg, $x/d = 1.5$ cal, alt = 100,000 ft).

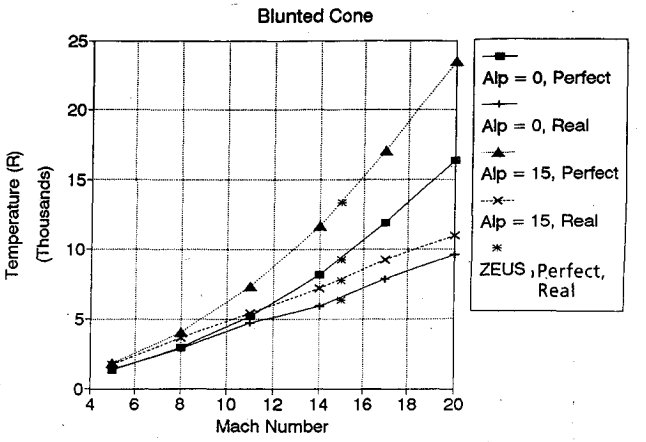

Fig. 12c Temperature predicted by approximate method on a 20% blunt cone as a function of Mach number ($M_\infty = 15$, $\Phi = 180$ deg, $x/d = 1.5$ cal, alt = 100,000 ft).

have the physics included for detailed interaction effects. These effects could include bow shock waves intersecting fins or fin shock waves intersecting the body. These interaction effects can cause local "hot" spots, and more detailed analysis codes such as ZEUS or Navier-Stokes solvers are required. The fin interaction effects are shown by the ZEUS results at $x = 9$ calibers to the end of the body.

The emphasis to this point has been on accurate values of inviscid surface temperature to allow accurate heat transfer analysis. In getting accurate values of heat transfer, accurate values of pressure prediction were required. These accurate values of pressure prediction also give good force and moment predictions. Figure 15 illustrates force and moment predictions as a function of angle of attack compared with the ZEUS code for the same configuration of Fig. 14. Note that the axial force only includes wave drag since ZEUS at present is an inviscid code. Accuracies on wave drag and normal force are within 10%, and center of pressure near angle of attack zero within 6% of the body length compared with the full Euler code. About half of the error in wave drag is due to the high fin alone predictions using the present strip theory approach, Fig. 15a. Note that the theory does predict some slight changes in forces and moments due to real gas effects. However, except for very specialized problems, it is believed that these effects can be neglected, particularly in an engineering code such as the aeroprediction code. However, as already noted many times, heat transfer analysis definitely needs to consider the real gas effects when flying at any appreciable time above $M_\infty = 6$–8.

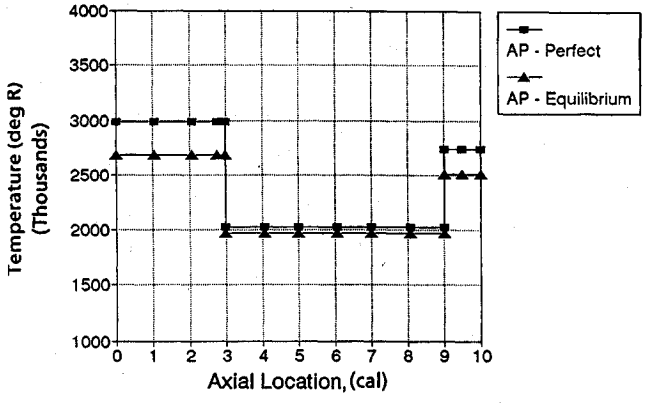

Fig. 13 Temperature distribution on a 10-deg cone-cylinder-flare configuration ($M_\infty = 15$, $\alpha = 10$ deg, $\Phi = 180$ deg).

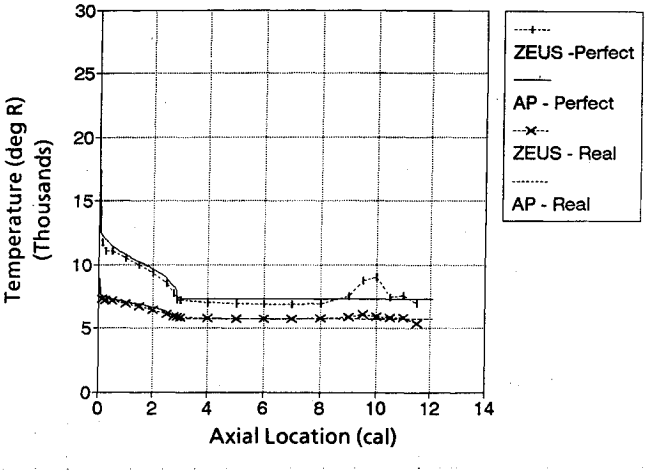

Fig. 14 Comparison of temperature predictions on a 20% blunt von Kármán ogive-cylinder-fin configuration ($M_\infty = 15$, $\alpha = 10$ deg).

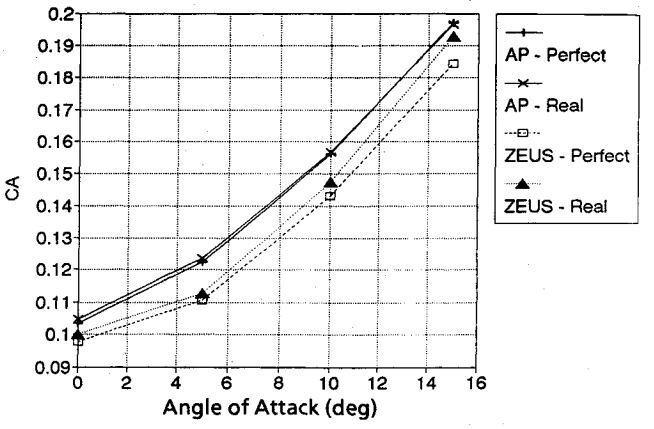

Fig. 15a Axial wave drag of a 20% blunt von Kármán ogive-cylinder-fin configuration ($M_\infty = 15$).

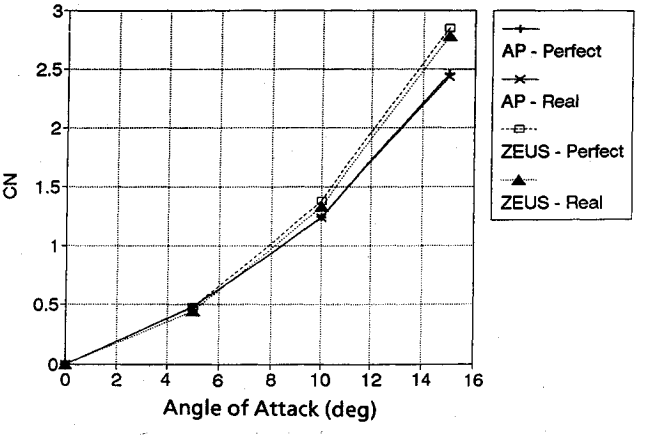

Fig. 15b Normal force coefficient of a 20% blunt von Kármán ogive-cylinder-fin configuration ($M_\infty = 15$).

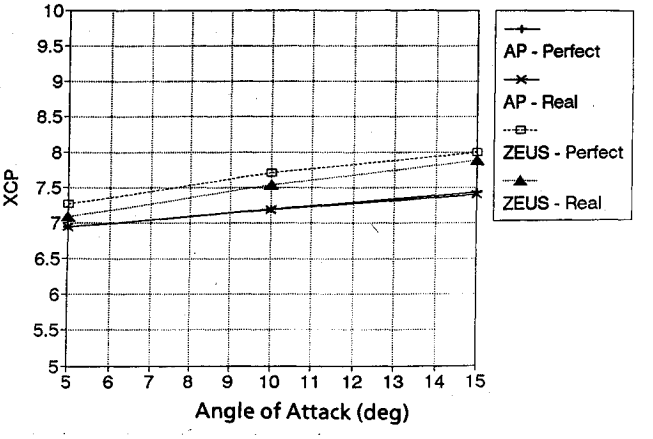

Fig. 15c Center of pressure of a 20% blunt von Kármán ogive-cylinder-fin configuration ($M_\infty = 15$).

Summary

New methods have been developed to compute inviscid surface pressures and temperatures for both perfect and equilibrium chemically reacting flows on both pointed and blunt bodies of revolution. These new methods include an improved shock-expansion theory, an improved MNT, and an improved method for angle-of-attack effects. Comparison of these approximate engineering techniques to numerical inviscid computations using a full Euler code showed the following: 1) agreement on the critical windward plane inviscid tempera-

tures generally of 4% or better, 2) agreement of inviscid surface temperatures of 10% or better, and 3) agreement of axial wave drag and normal force of 10%, and center of pressure 8% of body length. For the body alone, wave drag estimates are generally within 5% of full Euler computations.

A new real gas formulation for pressure gradient behind a corner was derived. However, in implementing this into the SOSET, it was found to be of little value. This is because at high Mach numbers, the exponential decay term used in the SOSET becomes positive, requiring SOSET to revert back to either GSET or TCT. It was shown that neither of these theories was best for all cases, and as a result, a user input to allow a choice of which method to use was considered the best alternative for use of the traditional SOSET.

With the new technology developed, the NSWCDD aeroprediction code can now be used to give engineering estimates of inviscid surface temperature for high Mach numbers. These approximate temperatures can then be used as inputs for more detailed heat transfer analysis.

Acknowledgments

Appreciation is expressed to Robin Staton and Dave Seigel, who manage and sponsor, respectively, the Surface-Launched Weapons Technology Block program. Without funding provided by this program, this new work would not have been possible. Appreciation is also given to Francis Priolo, who performed the ZEUS code computations for comparison with the present new approximate theories, and to Roy McInville for consultation on heat transfer requirements and techniques.

References

[1]Moore, F. G., "Body Alone Aerodynamics of Guided and Unguided Projectiles at Subsonic, Transonic, and Supersonic Mach Numbers," NWL TR-3796, Dahlgren, VA, Nov. 1972.

[2]Moore, F. G., and McKerly, B., "Aerodynamics of Guided and Unguided Weapons: Part I—Theory and Application," Naval Weapons Lab. TR-3018, Dahlgren, VA, Dec. 1973.

[3]Moore, F. G., and Swanson, R., "Aerodynamics of Tactical Weapons to Mach Number 3 and Angle ofAttack 1-5 Degrees: Part I—Theory and Application," Naval Surface Warfare Center, NSWC TR-3584, Dahlgren, VA, Feb. 1977.

[4]Devan, L., Mason, L., and Moore, F. G., "Aerodynamics of Tactical Weapons to Mach Number 8 and Angle of Attack 180," AIAA Paper 82-0250, Jan 1982.

[5]Moore, F. G., "Computational Aerodynamics at NAVSWC: Past, Present, and Future," Naval Surface Warfare Center, NAVSWC TR 90-569, Dahlgren, VA, Oct 1990.

[6]Park, C., and Loon, S., "Calculation of Real-Gas Effects on Blunt-Body Trim Angles," AIAA Paper 89-0685, Jan. 1989.

[7]Hender, D. R., "A Miniature Version ofthe JA70 Aerodynamics Heating Computer Program, H 800 (MINIVER)," McDonnell Douglas, MOC G0462 (COSMIC Program 3 MFS and 20951), June 1970.

[8]Moore, F. G., Armistead, M. A., Rowles, S. H., and DeJarnette, F. R., "Second-Order Shock-Expansion Theory Extended to Include Real Gas Effects," Naval Surface Warfare Center, NAVSWC TR 90-683, Dahlgren, VA, Feb 1991.

[9]Hudgins, H. E., Jr., "Supersonic Flow About Right Circular Cones at Zero Yaw in Air at Chemical Equilibrium, Part I—Correlation of Flow Properties," Picatinny Arsenal, TM 1493, Aug 1965.

[10]Heims, S., "Prandtl-Meyer Expansion of Chemically Reacting Gases in Local Chemical and Thermodynamic Equilibrium," NACA TN 4230, March 1958.

[11]Ames Research Staff, "Equations, Tables, and Charts for Compressible Flow," NACA TR 1135, 1953.

[12]Wittliff, C. E., and Curtis, J. T., "Normal Shock Wave Parameters in Equilibrium Air," Cornell Aero Lab Rept. CAL-III, Nov. 1961.

[13]Tannehill, J. C., and Mugge, P. H., "Improved Curve Fits for the Thermodynamic Properties of Equilibrium Air Suitable for Numerical Computation Using Time-Dependent or Shock-Capturing Methods," NASA CR-2470, 1974.

[14]Srinivasan, S., Tannehill, J., and Wielmuenster, K., "Simplified Curve Fits for the Thermodynamic Properties of Equilibrium Air," Engineering Research Inst., Iowa State University, Rept. ISU-ERI-AMES 86401, Ames, IA, Jun 1986.

[15]Morrison, A. M., Solomon, J. M., Ciment, M., and Ferguson, R. E., *Handbook of Inviscid Sphere-Cone Flow Fields and Pressure Distributions,* Volume I, NSWC/WOL/TR 75-45, Silver Spring, MD, Dec. 1975.

[16]DeJarnette, F. R., Ford, C. P., and Young, D. E., "A New Method for Calculating Surface Pressures on Bodies at an Angle of Attack in Supersonic Flow," AIAA Paper 79-1552, July 1974.

[17]Jones, D. J., "Numerical Solutions of the Flow Field for Conical Bodies in a Supersonic Stream," National Research Council of Canada, Rept. LR-507, July 1968.

[18]Priolo, F. J., Wardlaw, A. B., Jr., and Kuhn, G. D., "High Temperature Effects for Missile-Type Bodies Using the Euler Solver, ZEUS," AIAA Paper 91-3259, Sept. 1991.

Jerry M. Allen
Associate Editor